ELSEVIER

Journal of Nuclear Materials 297 (2001) 97–106

journal of nuclear materials

www.elsevier.com/locate/jnucmat

What's new on plutonium up to 4000 K?

M. Boivineau *

Commissariat à l'Énergie Atomique, Centre de Valduc, Département de Recherches sur les Matériaux Nucléaires, F-21120 Is-sur-Tille, France

Received 12 December 2000; accepted 5 March 2001

Abstract

The thermophysical properties of both solid and liquid plutonium have been investigated up to 4000 K and 0.12 GPa by use of the isobaric expansion experiment (IEX). Electrical resistivity, volume expansion (density), enthalpy, sound velocity, and equation of state parameters (bulk modulus, adiabatic and thermal compressibility, Grüneisen parameter, and the specific heat ratio) have been measured and extended in the whole liquid region up to nearly 4000 K, and are reported in this paper. Among numerous anomalies of Pu, the literature data have revealed that liquid Pu shows an atypical behavior by presenting a positive temperature coefficient for sound velocity up to 1225 K. We have confirmed such a behavior but also reported a drastic change of sound velocity at around 2000 K. Such results are interpreted in terms of the delocalization of the 5f electrons in liquid Pu.

1. Introduction

Studies on actinides have been limited because of their radioactive properties, which need specific work conditions. The latter become even more complicated when studying the liquid state because they are strongly corrosive metals (and especially Pu). In addition to these problems of corrosion (and consequently contamination with the container), conventional heating static techniques are not often well suited for measuring thermophysical properties of liquids at high temperature because of the thermal and radiative losses, evaporation (for high vapor pressure materials), and are then limited to low melting point materials. To overcome these difficulties and to reach higher temperature range, contactless techniques coupled with pulse heating techniques have been developed in the 1970s and successfully applied on liquid metals (including refractory metals) by a few laboratories ([1], and references therein).

This paper deals with the thermophysical properties of both solid and liquid plutonium. Although numerous data have been reported on solid Pu, studies on liquid Pu are rather sparse. We have particularly focused our attention onto sound velocity measurements, which are very useful for determining the equation of state (EOS) parameters of liquid metals [2–4]. As for the solid state which presents numerous anomalies (volume contraction of the δ phase, highest number of allotropic phases (6) of elements, monoclinic phase at ambient conditions, martensitic transformations, low heat of fusion, contraction on melting,...), liquid Pu shows an atypical behavior that will be discussed in this paper.

2. Experimental procedure and data evaluation

Our experimental device, commonly called isobaric expansion experiment (IEX), was first described in [5], then detailed in [6] with sound velocity measurements, and is schematically presented in Fig. 1. Briefly, the experiment consists in resistively pulse heating metallic wires (typically 1 mm diameter, 30 mm long) by discharging a 60 kJ capacitor bank (20 kV, 30 kA, 300 μF) in about 100 μs. The sample is located in an argon gas-filled pressure vessel, most of the experiments being carried out here around 0.12 GPa. Wire-shaped elec-

* Tel. +33-3 80 23 41 62; fax: +33-3 80 23 52 82.
E-mail address: michel.boivineau@cea.fr (M. Boivineau).

0022-3115/01/$ - see front matter
PII: S0022-3115(01)00549-9

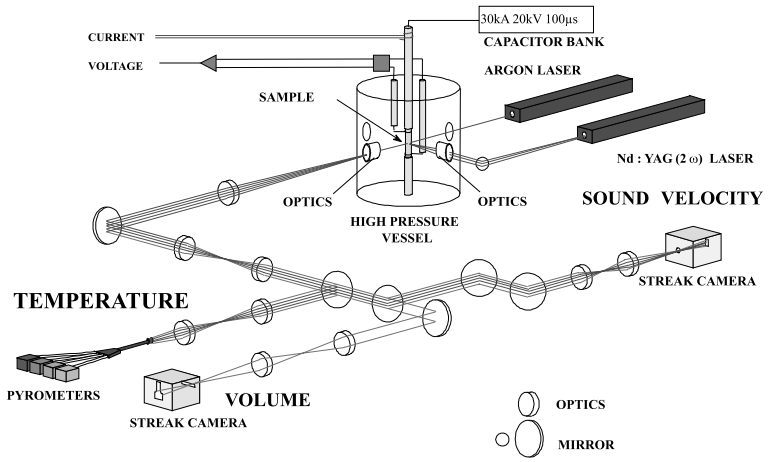

Fig. 1. Schematic diagram of the IEX.

Table 1
Main impurities in plutonium samples (ppm by weight)

Element	Al	Am	Cr	Cu	Fe	Ga	Ni
Content	80	>30	13	23	35	40	20

trorefined plutonium samples, whose typical chemical composition is given in Table 1, were specifically prepared in our laboratory. The sum of impurities, corresponding to a 53-element analysis, is 480 ppm weight.

At any period of time, the following basic measurements are available: (i) current intensity through the sample $I(t)$; (ii) voltage drop across the sample $U(t)$; (iii) diameter of the sample $\phi(t)$; and (iv) thermal emission from the heated sample $J(t)$. The current, voltage, and diameter are measured with an accuracy of $\pm 0.6\%$, $\pm 0.6\%$ and $\pm 1.5\%$, respectively.

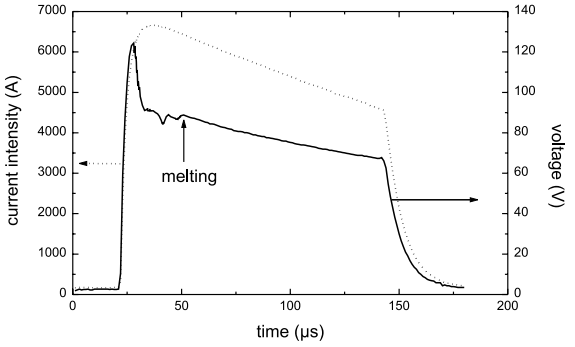

Fig. 2. Electrical measurements (bank voltage $U_B = 6500$ V: current pulse ~ 120 µs) for a plutonium sample ($\phi_0 = 0.92$ mm). Full curve: voltage measurements. Dotted curve: current intensity.

Typical electrical measurements such as current intensity and voltage are shown in Fig. 2 for a plutonium sample. Strong variations of voltage measurements clearly indicate phase transformations in solid and liquid Pu. These data are then used for calculating enthalpy and electrical resistivity with Eqs. (1) and (3) (see below).

From these measured quantities mentioned above, thermophysical parameters, namely, enthalpy $H(t)$, electrical resistivity $\rho_{el}(t)$, specific volume $V/V_0(t)$ (and consequently density), and temperature $T(t)$ are calculated. By combining these different terms (which are all reported as a function of time), one obtains $H(T)$, $\rho_{el0}(T)$, $\rho_{el0}(H)$, $\rho_{el}(T)$, $\rho_{el}(H)$, $V/V_0(T)$, $V/V_0(H)$, and the specific heat at constant pressure C_p as shown in Fig. 3. Electrical resistivity, specific volume and enthalpy are measured with an accuracy of $\pm 4\%$, $\pm 3\%$ and $\pm 1.5\%$, respectively.

Due to the isobaric conditions, and according to the second law of thermodynamics, the enthalpy is equal to the internal energy, and thus to the electrical power (Joule effect). Then we have

$$\Delta H = H(T) - H(298) = \frac{1}{m}\int_{t_0}^{t} I(t)U_c(t)\,dt, \tag{1}$$

where m is the mass of the sample, and U_c is the voltage corrected for the inductive term:

$$U_c(t) = U(t) - L\frac{dI(t)}{dt}, \tag{2}$$

where L is the self-inductance of the circuit.

The electrical resistivity is simply calculated from the Ohm's law:

$$\rho_{el0}(t) = \frac{U_c(t)}{I(t)}\frac{\pi\phi_0^2}{4l}, \tag{3}$$

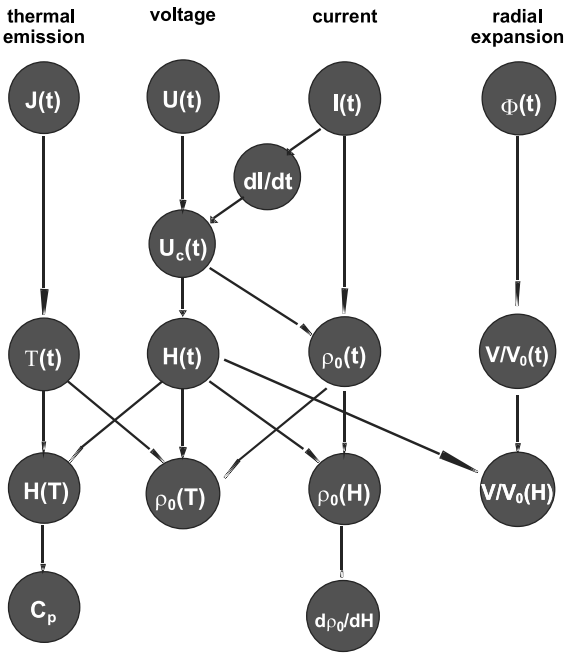

Fig. 3. Measured quantities and calculated parameters obtained from the IEX.

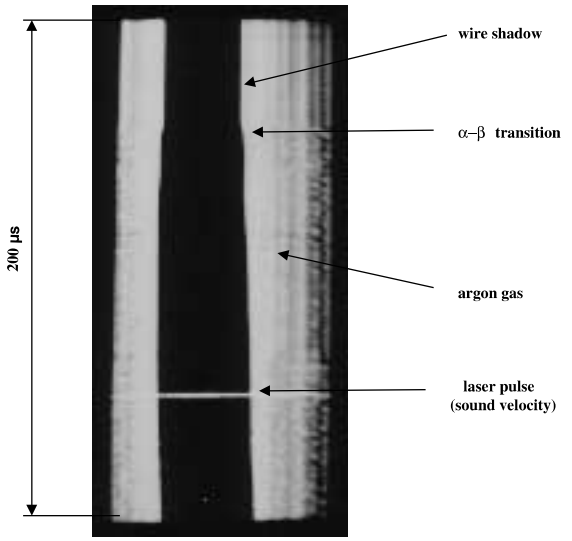

Fig. 4. Radial expansion image as a function of time.

where ϕ_0 is the initial wire diameter and l is the distance associated with the potential difference measurement.

The radial expansion, and consequently the volume variation, are obtained by employing a shadowgraph technique with the use of a streak camera. A continuous argon laser backlights the sample, whose shadow is transported onto the slit of the camera. Since supporting jaws block both ends of the wire, only radial expansion occurs.

A typical steak image is shown in Fig. 4 for a plutonium sample, which clearly indicates the α–β phase transformation due to its strong expansion (linear expansion $\Delta l/l \sim 3\%$). Such an image is then treated by image processing and provides the relative radial expansion variation $\phi(t)/\phi_0$. Since the sample remains as a solid and then a liquid column (the geometrical symmetry being then preserved) during heating (before collapsing after the end of the experiment due to the gravity), the specific volume is then calculated from the following expression:

$$\frac{V(t)}{V_0} = \frac{\phi(t)^2}{\phi_0^2}. \tag{4}$$

The density ρ (or specific gravity) can be then calculated by using the mass conservation law as follows:

$$\rho = \rho_0 \frac{V_0}{V(t)}, \tag{5}$$

where ρ_0 is the initial density of the sample (19 860 kg/m^3 for Pu-α).

The correct electrical resistivity ρ_{el} must take into account the radial expansion of the wire during heating. Then Eq. (3) becomes

$$\rho_{el}(t) = \frac{U_c(t)}{I(t)} \frac{\pi\phi(t)^2}{4l} = \rho_{el0}(t) \frac{\phi(t)^2}{\phi_0^2}. \tag{6}$$

Multispectral optical pyrometry is also commonly used in our laboratory for measuring temperature, especially for liquid refractory materials (see [5]). However, the observation of the melting plateau is needed in order to get accurate measurements. Indeed, this need comes from the calculation of an instrumental factor (named G_i in [5], and which includes different kinds of losses) at the melting point, which is then extrapolated in the whole temperature range of the liquid. Therefore, for plutonium, temperature measurements are difficult to perform with such a technique, because of its low melting point ($T_M = 913$ K) far below the threshold of our pyrometers (~1500 K), meaning the melting plateau is not observed. However, due to our highly precise enthalpy measurements (±1.5%) and the very accurate and reproducible $C_p = 177$ J kg^{-1} K^{-1} recommended value of specific heat at constant pressure (isobaric conditions) by Oetting et al. [7], temperature measurements have been rather obtained by using the general expression

$$\Delta T = \frac{\Delta H}{C_p} \tag{7}$$

and then especially applied for the *liquid* phase:

$$T = T_M + \frac{(H - H_M)}{C_p}, \tag{8}$$

where T_M is the melting temperature ($T_M = 913$ K), [1] $H_M = 130$ J g^{-1} the enthalpy value at the start of the liquid phase (see Section 3.1), and H is the total energy determined by Eq. (1). It should be also noted that C_p is assumed to be constant ($C_p = 177$ J kg^{-1} K^{-1}) in the whole temperature range of the liquid, which is a general trend for most of the liquid metals. In such a way, the temperature incertitude should not exceed ±5% in the liquid. Eq. (7) was also used for the solid phase by using the average value of both the available data of Oetting and Adams [8], and Rollon and Gallegos [9].

Sound velocity measurements have been developed to provide EOS parameters such as the adiabatic B_S and isothermal B_T bulk moduli and the corresponding compressibility χ_S and χ_T, the Grüneisen parameter γ_G, and the specific heat ratio γ.

The principle of creating sound waves, shown in Fig. 5, consists in focusing a doubled frequency Nd:YAG ($\lambda = 532$ nm) Q-pulsed laser onto a spot on one side of the sample. The resulting instantaneous stress wave ($t = 0$: see Fig. 5(a)), which is spherically diverging and degrading into an acoustic pulse, propagates through the sample and emerges on the side opposite the laser source. The consecutive small amount of surface motion generates disturbances into the surrounding argon gas, corresponding to the propagation of the resulting acoustic waves in the pressure medium. Such disturbances are clearly displayed by the observation of 'shadows' in the gas (correlated to changes of density) when using a streak camera (see Fig. 5(b)). The arrival time of the acoustic wave, propagating through the sample diameter, is then determined at the emergence time of the wave starting from the sample side opposite the laser pulse. This time is calculated from the streak image (vertical scale), and sound velocity is deduced when knowing the diameter value (which is known from radial expansion image: see Fig. 4). Such a value is calculated at the laser pulse arrival, the latter being shot when temperature remains constant after the end of the current pulse (no more electrical energy).

The main advantage of such a method compared with interferometric techniques which were initially used for a similar experimental device than ours [10], is to get rid of surface motions of the liquid which causes a displacement of the reflected probe laser allowing the observation of the fringe shift in the interferometer due to the stress pulse.

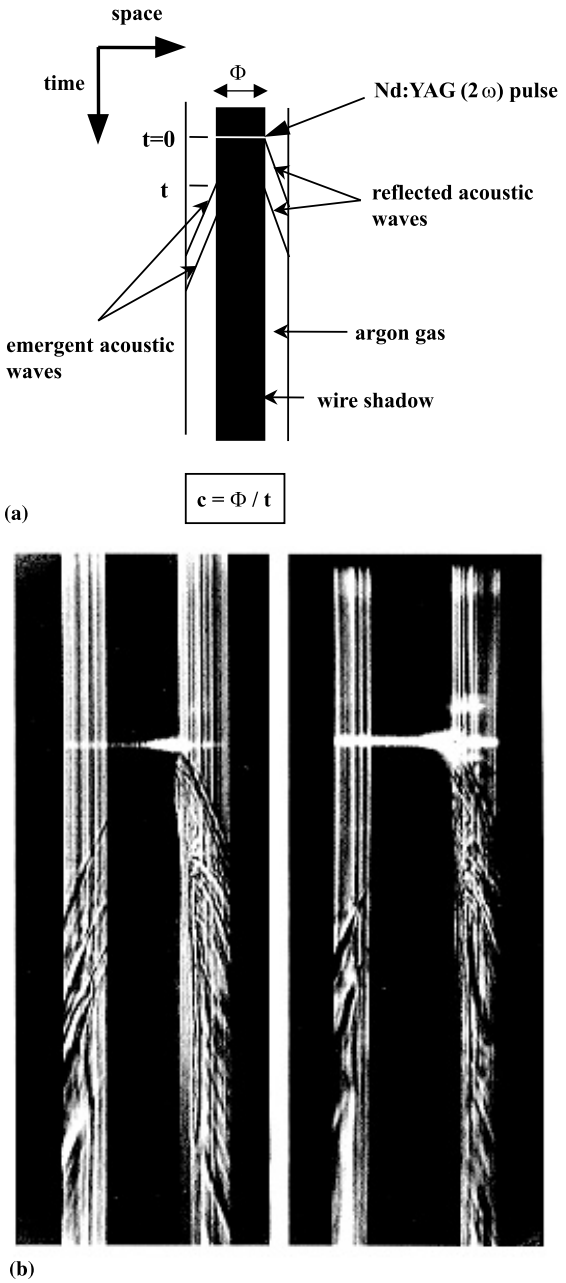

Fig. 5. Sound velocity measurements (a) principle of the determination of sound velocity correlated with pictures of Fig. 5(b), (b) typical images obtained with the streak camera devoted to sound velocity measurements. On the left, the sample remains at 300 K (no electrical energy). On the right, the sample is heated up to 2000 K. It can be noted that the acoustic wave arrival time is longer than for the previous experiment (300 K), meaning the sound velocity has changed.

The accuracy of sound velocity measurements strongly depends on the quality of the image and streak duration to well determine the time of the emergent

[1] Due to our low pressure ($P = 0.12$ GPa) experiments, and integrating our ±5% error bars, the ambient pressure melting temperature has been used here.

wave starting from the sample opposite the laser source. Typically, it is found to be around ±5%.

Assuming an isotropic and homogeneous solid material, sound velocity c_s is usually defined as follows:

$$c_s = \left(c_L^2 - \tfrac{4}{3}c_T^2\right)^{1/2}, \tag{9}$$

where c_L is the longitudinal component and c_T is the shear component. Since such a method only gives access to c_L, it is then well suited for studying the liquid phase (the shear component being neglected then: $c_T \sim 0$) since one has

$$c_l = c_L, \tag{10}$$

where c_l is the sound velocity in the liquid phase. Liquid EOS parameters are then determined from Eq. (10), namely, adiabatic and isothermal compressibility χ_S and χ_T, defined as a consecutive volume variation due to pressure at constant entropy and temperature, respectively, may be determined from the knowledge of sound velocity c and density ρ. For convenience, one introduces the adiabatic B_S and isothermal B_T bulk moduli, inversely equal to their corresponding compressibility, and defined as follows:

$$B_S = \frac{1}{\chi_S} = -V\left(\frac{\partial P}{\partial V}\right)_{S=cst} = \rho\left(\frac{\partial P}{\partial \rho}\right)_{S=cst} = \rho c^2. \tag{11}$$

By using Eqs. (9) and (10), we have then for solids:

$$(B_S)_s = \rho(c_L^2 - \tfrac{4}{3}c_T^2) \tag{12}$$

and for liquids:

$$(B_S)_l = \frac{1}{\chi_S} = \rho c_L^2 = \rho c_l^2. \tag{13}$$

χ_S, χ_T, B_S, and B_T are related by the following expression:

$$\frac{B_S}{B_T} = \frac{\chi_T}{\chi_S} = \gamma, \tag{14}$$

where γ is the specific heat ratio and expressed by

$$\gamma = \frac{C_p}{C_v} = 1 + T\frac{\alpha^2 c^2}{C_p}, \tag{15}$$

where C_p and C_v are the specific heats at constant pressure and volume, respectively, T is the absolute temperature (in K). The volume thermal expansion coefficient α, determined from the usual IEX data (see above), is defined by

$$\alpha = \frac{1}{V}\left(\frac{\partial V}{\partial T}\right)_P. \tag{16}$$

Grüneisen's gamma γ_G, linking pressure on the sample to its internal energy, is also commonly used and is expressed by

$$\gamma_G = V\left(\frac{\partial P}{\partial E}\right)_V = \alpha\frac{c^2}{C_p}. \tag{17}$$

By combining Eqs. (15) and (17) one finds

$$\gamma = 1 + T\alpha\gamma_G. \tag{18}$$

The Poisson coefficient can be also obtained by introducing the $k = c_L/c_T$ ratio:

$$\sigma = \frac{k^2 - 2}{2(k^2 - 1)}. \tag{19}$$

Eq. (19) is obviously valid for the solid state but not in the liquid since $c_T = 0$.

3. Results and discussion

Results on electrical resistivity (Section 3.1), volume variation (Section 3.2), and sound velocity (Section 3.3) are presented and discussed.

3.1. Electrical resistivity

The electrical resistivity of Pu has been studied under rapid heating conditions in the 8×10^6–6×10^7 K s^{-1} range. Results are reported in Fig. 6 as a function of enthalpy for solid Pu at two different pressures (P_{atm} and 0.2 GPa). At ambient pressure, one can easily distinguish the six allotropic phases of solid Pu (except for the γ phase) before melting, by exhibiting the variations of electrical resistivity, as previously observed ([11], and references therein). The structural stability of each phase at P_{atm} is indicated in Fig. 6 by vertical lines with the corresponding heat of phase transformation.

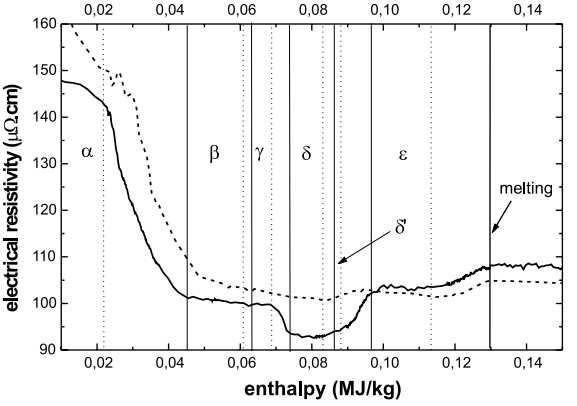

Fig. 6. Electrical resistivity versus enthalpy of pure solid plutonium at P_{atm} (full curve) and 0.2 GPa (dashed curve). The phases and enthalpies of transformation are indicated for $P = P_{atm}$ by vertical lines: the full lines and the dotted lines indicate the start and the end of the allotropic phases, respectively.

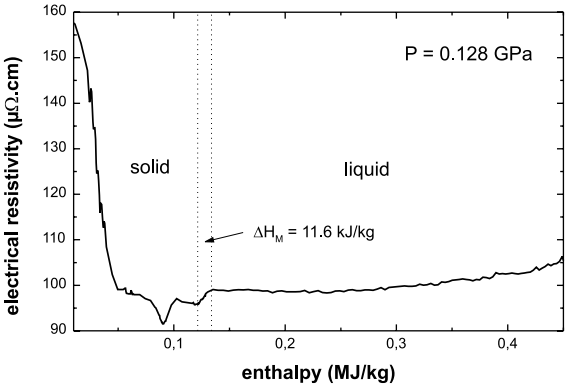

Fig. 7. Electrical resistivity versus enthalpy of pure solid and liquid plutonium at 0.128 GPa (bank voltage $U_B = 5600$ V; $\phi_0 = 0.92$ mm).

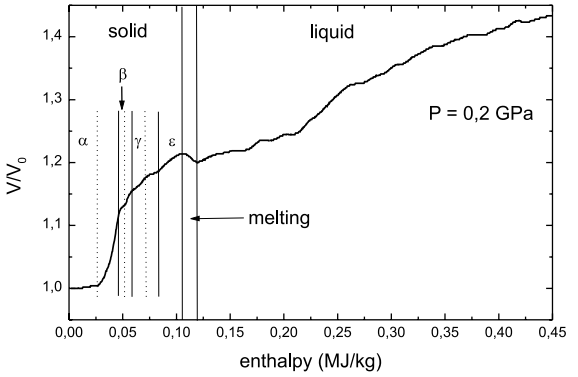

Fig. 8. Relative volume versus enthalpy of Pu at 0.2 GPa. The phases and enthalpies of transformation are indicated by vertical lines: the full lines and the dotted lines indicate the start and the end of the allotropic phases, respectively.

The main conclusions of this study are given as follows:

- the allotropic transition temperatures are systematically and significantly *higher* than the static measurements (46, 70, and 20 K for the α–β, γ–δ and δ–ε phases, respectively);
- the transition start temperatures do not depend on the heating rate;
- the β–γ transition is not well observed as for static data [11];
- the 130 kJ kg^{-1} enthalpy value for reaching the *liquid* state is the same as static data, and is *independent* of the heating rate;
- by analyzing both curves, it can be noted that δ and δ′ phases disappear at 0.2 GPa, which is consistent with the different available P–T phase diagrams reported in the literature [12–15].

The major interest of the IEX concerns the study of *liquid metallic materials* (including refractory metals). Then, electrical resistivity measurements have been performed in the high temperature range of the liquid phase, as shown in Fig. 7 at $P = 0.128$ GPa. The comments on these results are the following:

- the present experiment corresponds to a 446 kJ kg^{-1} total enthalpy, i.e., $T_{max} \sim 2700$ K from Eq. (8);
- the electrical resistivity is nearly constant (∼100 μΩ cm) in the whole liquid phase;
- the *heat of fusion* was found to be 11.6 kJ kg^{-1}, in very good agreement with the 11.75 kJ kg^{-1} recommended literature data [8].

3.2. Specific volume

The volume variation of Pu up to the liquid state has also been studied, and is calculated from Eq. (4) after having analyzed the streak radial expansion image (see Fig. 4). Results are shown in Fig. 8, the experiment being carried out at 0.2 GPa. Such measurements lead to the following comments:

- a very good agreement is observed with electrical resistivity measurements;
- the α–β transition is clearly exhibited, and is accompanied by a 12.7% volume variation, compared with the 9% admitted value from the 3% linear expansion measurements [11,14,16,17];
- as for the electrical resistivity, the δ and δ′ are not observed at 0.2 GPa in agreement with the literature P–T phase diagrams;
- as observed in previous works [18], the volume contraction at melting is well evidenced;
- the volume expansion monotonously increases in the liquid state. The best linear fit of our data was found to be 11×10^{-5} K^{-1}, in good agreement with the 9×10^{-5} K^{-1} averaged value reported in [18].

3.3. Sound velocity and EOS parameters

As mentioned in Section 2, this device is particularly well suited for the liquid state regarding the sound velocity measurements, since such a laser generated method only gives access to the longitudinal component (the shear mode is considered to be neglected in the liquid). This is then the main reason for having focused our attention onto the liquid state. However, this technique was first qualified in solid Pu with a very good agreement with Calder et al. results [19] regarding the α phase, and we have confirmed previous data [20] by observing changes of sound velocity corresponding to the, β, γ, δ′ (not δ) and ε phases as shown in Fig. 9 for two different pressures (0.05 and 0.12 GPa). Temperature is indicated (but not measured) here on the top of Fig. 9.

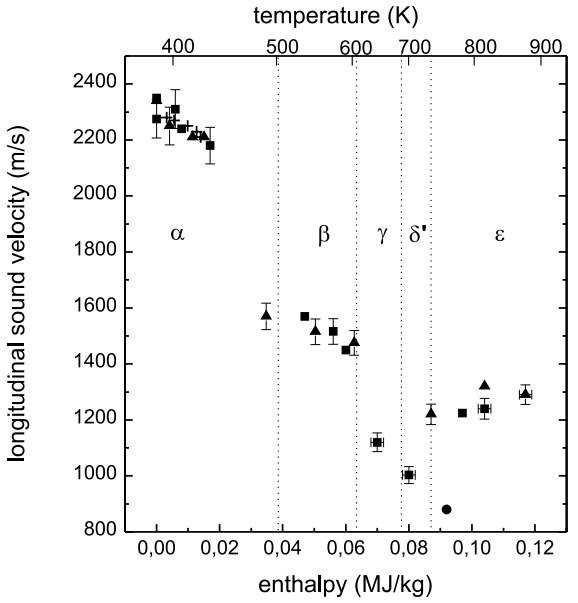

Fig. 9. Longitudinal sound velocity in solid Pu. (■) $P = 0.12$ GPa. (▲) $P = 0.05$ GPa. (●) Ref. [21].

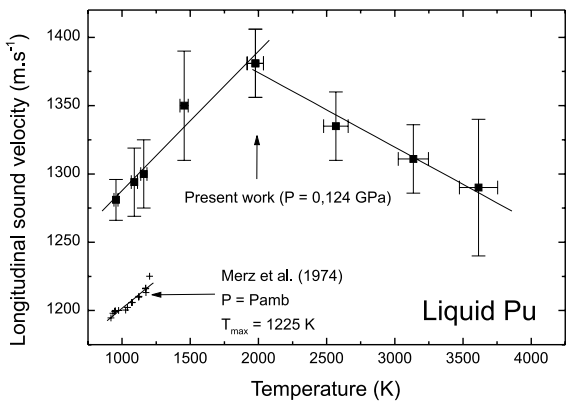

Fig. 10. Longitudinal sound velocity in liquid Pu. (■) present work. (+) Ref. [22].

These results are summarized as follows.

- A strong variation of longitudinal velocity is observed from α (∼2200 m/s) to β (∼1550 m/s).
- Whereas β and γ phases present close electrical resistivity values, they exhibit a drastic 300 m/s drop of sound velocity (from 1500 down to 1200 m/s) at the transition.
- The 1000 m/s value of the δ′ phase is particularly low.
- The ε phase indicates a nearly constant value (∼1230 m/s). However, a significant dispersion of data has been observed by comparing our results with those of Cornet and Bouchet [21]. Indeed, their results at 758 K and ambient pressure indicate $\sigma = 0.2$ and $B_S = 6.26$ GPa values. By considering their reported Poisson coefficient and using Eq. (19), this would lead to a $k = 1.63$ value, and then $c_T = 753$ m/s when taking our 1230 m/s (at $P = 0.12$ GPa) longitudinal sound velocity. Combining both components, the bulk modulus is found to be $B_S = 12.3$ GPa, i.e., nearly twice the 6.26 GPa value. Such a discrepancy cannot be due to the effect of pressure since close measurements (∼1230 m/s for the longitudinal velocity) were also found at $P = 0.05$ GPa.
- Anyway, the bulk modulus value is very low and similar to soft liquid metals (e.g., Li or Na). Moreover, ε-Pu looks like a liquid, which is reflected throughout its low 11.6 kJ kg^{-1} heat of fusion.

As mentioned before, we have investigated and focused our attention on the liquid state, whose results are reported in Fig. 10. Only a few reported data have been obtained in such a state, and in any case, for a low temperature range. Then, our results are compared here with the only available data obtained by Merz et al. [22] regarding the sound velocity in liquid Pu.

Our study has consisted in extending the temperature range in the whole liquid state of Pu up to nearly 4000 K. Results are shown in Fig. 10 and lead to some comments.

- For the same temperature range (up to 1225 K), we have confirmed the positive temperature coefficient, meaning sound velocity *increases* as a function of temperature. This is an atypical behavior that is discussed in detail below. This phenomenon occurs up to 2000 K prior to a drastic change of slope (decrease of sound velocity) up to nearly 4000 K.
- Our values are around 80 m s^{-1} higher than those of Merz et al. [22]. Such a difference may be explained by the difference of pressure (0.124 GPa for this work and ambient pressure for Merz et al.). Indeed, the effect of pressure is associated with a decrease of compressibility, and then an increase of sound velocity.
- Even within our higher uncertainties (±5%), the slopes are in very good agreement: 0.08 m s^{-1} K^{-1} for Merz et al. [22], and 0.1 m s^{-1} K^{-1} for this work.
- By precisely measuring the enthalpy, temperature values have been calculated by using Eq. (8). The error on temperature is estimated by assuming a reasonable incertitude on C_p of ±10 J kg^{-1} K^{-1}.

The most remarkable fact of these results is related to the increase of sound velocity with temperature. Such an observation is considered to be *anomalous* since most of the materials present a negative temperature coefficient. A specific attention onto these atypical cases shows a correlation with a *volume contraction on their melting point* [23]. It should be then noted that the reported examples are mainly semimetals such as Bi, Sb, Ge, Si, Ga, Te [24–27], in addition to H_2O [28]. For all of these cases, the volume contraction is associated to a negative

slope of the melting curve according to Clausius–Clapeyron's law [2] [18].

Concerning the f elements (lanthanides and actinides), Ce and Pu are known to exhibit a volume contraction too, as reflected through the negative slope of their melting curve prior to a minimum (3.3 GPa for Ce [29], and 4 GPa for Pu [15]) and a positive slope. As for the materials mentioned above, it was then shown that sound velocity increases for liquid Ce and Pu up to the reported upper temperature limits (1500 K for Ce [30], and 1225 K for Pu [22]). For both cases, the volume contraction, and consequently the rise of sound velocity, are interpreted as an effect of the hybridization, of 4f and 5f electrons with the 5d6s and 6d7s conduction band of Ce and Pu, respectively. Such a phenomenon would occur on melting and further up in the liquid state. For the case of Pu, the body-centered cubic (bcc) structure ε phase existing prior to melting, for which the 5f electrons are rather localized, would be then replaced by a lower symmetry (random structure) and a denser liquid phase where the participation in bonding of the so-called delocalized (or itinerant) 5f orbitals would be predominant. Such a contribution is due to the broadening and lowering of the 5f wave functions which consequently form overlapping energy bands with the 6d7s conduction shell.

From a general point of view, the 5f electrons are known to play a major role in the actinide metal series (corresponding to the progressive filling up of the 5f electronic sub-shell), and are the consequence of its separation in two sub-series. The first one corresponds to the *light* actinides and ranges from protactinium to plutonium, which presents a nearly parabolic decrease in atomic radii with atomic number (close to that of the 5d transition metals) [31]. Such an observable fact provides a convincing evidence that the 5f sub-shell do bond as valence electrons, causing the increase of cohesion and then a decrease of the atomic volume. Moreover, it is consistent with the observation of the decrease of the crystal lattice symmetry (due to the highly anisotropic character of the 5f electrons bonds) and the increase of the structure number from Pr to Pu, as exhibited throughout the interconnected phase diagrams of binary actinides alloys [32]. Then, Pu is the most complex element and has the lowest structural symmetry at ambient conditions (monoclinic, 16 atoms per unit cell), and the highest number (6) of allotropic transitions as a function of temperature. A drastic jump of the atomic radius is then observed from Pu to Am, the latter starting the second series which behaves more like the rare-earths (corresponding to the progressive filling up of the 4f electronic sub-shell), as shown through their nearly constant atomic volume variation. Hence, as for rare-earths, where the 4f valence electrons are localized in the ionic core (and then chemically inert and presenting local magnetic moments), the 5f are supposed to be rather localized for this second series. Such an observation is emphasized by the obtention of a higher symmetry for Am (dhcp = double hexagonal close packed type) and heavier actinides, and a lower number of allotropic phases as indicated in the interconnected phase diagrams of binary actinide alloys [32]. All of these mentioned phenomena are exhibited and compiled in [33] and [34].

The results on sound velocity measurements can be more easily understood and discussed in terms of compressibility, and more specifically of temperature coefficients. Indeed, both coefficients of sound velocity and adiabatic compressibility are related by the following expression:

$$\frac{1}{\chi_S}\left(\frac{d\chi_S}{dT}\right)_P = -\left(\frac{2}{c_L}\frac{dc_L}{dT} + \frac{1}{\rho}\frac{d\rho}{dT}\right) \tag{20}$$

by differentiating Eq. (13). When analyzing Eq. (20), it can be noted that, since the second term is nearly always negative [3] (positive by including the sign of Eq. (20)) and due to its very low value (because of the high density of Pu), the $d\chi_S/dT$ sign *only depends* on the sign of dc_L/dT (more precisely on $-dc_L/dT$). In the general case for liquid metals, $dc_L/dT < 0$ (and thus $-dc_L/dT > 0$), and then $d\chi_S/dT > 0$: this corresponds to a loosening of structure with increasing temperature. In the particular case of Pu (as well as the other cited anomalous materials), $d\chi_S/dT$ is then negative for $T_M < T < 2000$ and positive for $2000 < T < 4000$ K (see Fig. 10). Thus, for $T = 1500$ K ($\rho \sim 15380$ kg m^{-3}), $1/\chi_S(d\chi_S/dT)$ is found to be close to -1.5×10^{-4} K^{-1}, whereas at $T = 3150$ K ($\rho \sim 13000$ kg m^{-3}) it is found to be $+1.5 \times 10^{-4}$ K^{-1}.

From these considerations, the hybridization of the f electrons with the conduction band mentioned for Ce [4] and Pu, associated with an increase of the atomic cohesion (decrease of the interatomic distance) due to their bonding, would lead to a decrease of compressibility ($d\chi_S/dT < 0$) and then to an augmentation of sound velocity ($dc/dT > 0$).

Moreover, it should be pointed out that most of these cited anomalous materials present a maximum of sound

[2] On melting, the dP/dT sign only depends on ΔV since ΔH and T (in K) are always positive.

[3] The only exception of the Periodic Table being the δ and δ′ phases of Pu.

[4] Ce is an exception among the rare-earths regarding the role of the 4f electrons. Indeed, in addition to its contraction on melting, it presents the unique isostructural transition (γ(fcc)–α(fcc)) among the elements, operating at 0.75 GPa and 300 K and which would be interpreted as a Mott transition where the 4f electrons are rather localized and delocalized in the γ and α phases, respectively.

velocity (minimum of compressibility) as temperature increases, before exhibiting a negative temperature coefficient (normal behavior). Our laboratory has also shown such a behavior for Ce [35] at high temperature ($T_{max} \sim 2800$ K) far above the melting point ($T_m = 1071$ K), which was then not observed by McAlister and Crozier [30], because of their lower reported temperature range. This phenomenon has been attributed to a competition of two antagonist effects, i.e., the hybridization process and thermal motion that is probably predominant at high temperature. Indeed, the latter increases the interatomic distance which then increases the compressibility correlated to a decrease of sound velocity. In that case, cerium would find again a normal behavior and exhibits negative temperature coefficient of sound velocity. This tends to prove that thermal motion no longer allows delocalized f electrons to impose their character. This argument is of course extended and applied here to Pu, due to the strong similarities between both cases. Then, it was expected that Pu would behave like Ce.

At last, it should be noted that one should expect a normal behavior in the whole temperature range for pressure values higher than 4 GPa (minimum of the melting curve) because of a volume expansion at melting (no contraction would then occur), according to Clausius–Clapeyron's law for this very high pressure region.

As reminded above, sound velocity measurements are very useful for providing EOS parameter calculations (see Section 2). Then, the isothermal bulk modulus B_T, the Grüneisen parameter γ_G, and the specific heat ratio γ variations are reported in Figs. 11–13, respectively, at $P = 0.12$ GPa. These data are reported here as a function of density ρ (expressed in g cm^{-3}), with temperature indications.

It can be seen from Fig. 11 that the isothermal bulk modulus B_T is constant at 24 GPa from the liquid density down to a 15 value. Then, it linearly decreases with a

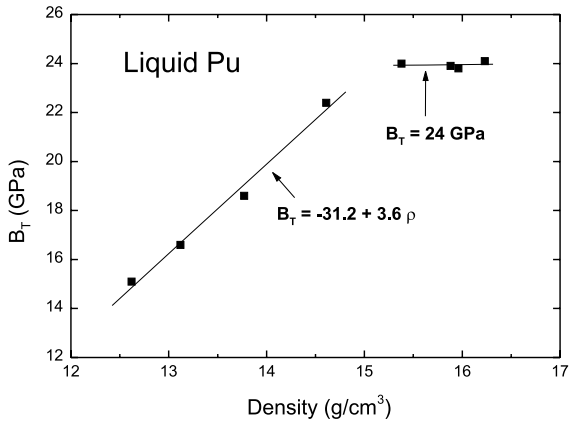

Fig. 11. Isothermal bulk modulus versus density in liquid Pu.

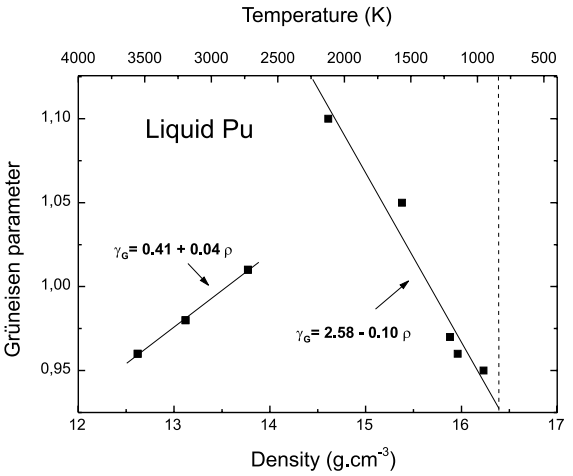

Fig. 12. Grüneisen parameter versus density in liquid Pu.

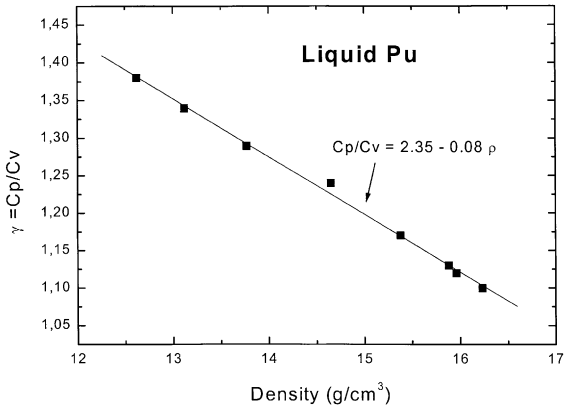

Fig. 13. Specific heat ratio versus density in liquid Pu.

3.6 GPa g^{-1} cm^3 coefficient with decreasing density (correlated to an increase of temperature).

The Grüneisen parameter variation versus density (see Fig. 12) presents a maximum at a density close to 15. The corresponding fits are $\gamma_G = 2.58 - 0.1\ \rho$ and $\gamma_G = 0.41 + 0.04\rho$ for the higher and lower density ranges. It can be noted that the $\gamma_G = 0.41$ value obtained by extrapolating the density down to zero (very high temperatures) is close to the 0.66 usual value observed for perfect monoatomic gases.

We have also reported the specific heats ratio $\gamma = C_p/C_v$ as a function of density as shown in Fig. 13. From a first sight, this parameter does not surprisingly present any drastic change as for other previous factors, but linearly decreases with density (and thus increases with temperature) according to: $\gamma = 2.35 - 0.08\rho$. The reason should be explained from Eq. (18): by reminding that the expansion coefficient is independent of

temperature (11×10^{-5} K^{-1}), and γ_G being of the order of unity, the second term $\alpha T \gamma_G$ is small compared to 1, and then does not strongly influence the value of γ. Due to this argument, the observation of a maximum for γ_G (ranging from 0.95 to 1.1: see Fig. 12) is not exhibited through the variation of γ.

4. Conclusion

This paper is a review of the thermophysical properties of both the solid and liquid states of Pu up to nearly 4000 K. We have focused our attention on the *liquid phase*, which is here the main novelty of this article regarding the literature data, because of a very low number of papers dealing with this topic.

We have shown that, as expected, liquid Pu exhibits an odd behavior regarding the results on sound velocity and EOS parameters. Such a phenomenon is interpreted as a delocalization process of the 5f electrons, and their consecutive participation to bonding.

We have also noted that a normal behavior should be expected in the whole temperature range for pressure values higher than 4 GPa (minimum of the melting curve). The observed maximum of sound velocity should shift to lower temperature values as pressure reaches 4 GPa, and should disappear above this value (normal behavior due to the absence of contraction on melting). New experiments at higher pressures could be performed in this way.

Acknowledgements

A special thanks to A. Berthault for having performed and interpreted previous studies. J.-M. Vermeulen, L. Arles and G. Toury are gratefully acknowledged for their technical participation in this work. J.-L.Truffier and Th. Thévenin are also thanked for helpful and lively earlier discussions, as P. Le Poac and M. Guillemot are for their critical reading of this manuscript.

References

[1] A. Cezairliyan, High Temp.–High Press. 11 (1979) 9.
[2] P. Kuchhal, R. Kumar, N. Dass, Phys. Rev. B 55 (1997) 8042.
[3] P. Ascarelli, Phys. Rev. 173 (1968) 271.
[4] G.M.B. Webber, R.W.B. Stephens, Phys. Acoust. IV-B (1968) 53.
[5] A. Berthault, L. Arlès, J. Matricon, Int. J. Thermophys. 7 (1986) 167.
[6] M. Boivineau, L. Arlès, J.M. Vermeulen, Th. Thévenin, Physica B 190 (1993) 31.
[7] F.L. Oetting, M.H. Rand, R.J. Ackermann, The Chemical Thermodynamics of Actinide Elements and Compounds, Part I, The Actinide Elements, IAEA, Vienna, 1976.
[8] F.L. Oetting, R.O. Adams, J. Chem. Thermodyn. 15 (1983) 537.
[9] C.E. Rollon, G.F. Gallegos, J. Therm. Anal. 21 (1981) 159.
[10] G.R. Gathers, J. Shaner, C.A. Calder, W.W. Wilcox, in: Proceedings of 7th Symposiuum on Thermophysical Properties, Gaithersburg, MD, USA, May 1977, ASME, New York, 1977.
[11] T.A. Sandenaw, J.F. Andrew, J. Nucl. Mater. 173 (1990) 59.
[12] D.R. Stephens, J. Phys. Chem. Solids 24 (1963) 1197.
[13] J.R. Morgan, in: W.N. Miner (Ed.), Plutonium 1970 and Other Actinides, New York, 1970.
[14] C.E. Olsen, J.F. Andrew, J. Nucl. Mater. 199 (1992) 6.
[15] C. Roux, P. Le Roux, M. Rapin, J. Nucl. Mater. 40 (1971) 305.
[16] B. Hocheid, A. Tanon, J. Miard, Acta Metall. 13 (1965) 144.
[17] W.N. Miner, F.W. Schonfeld, in: Wick (Ed.), Plutonium Handbook, Gordon and Breach, New York, vol. I, 1967.
[18] C.Z. Serpan, L.J. Wittenberg, Trans. Met. Soc. AIME 221 (1961) 1017.
[19] C.A. Calder, E.C. Draney, W.W. Wilcox, J. Nucl. Mater. 97 (1981) 126.
[20] A.E. Kay, P.T. Linford, in: E. Grison, W.B.H. Lord, R.D. Fowler (Eds.), Plutonium 1960, London, 1961.
[21] J.A. Cornet, J.M. Bouchet, J. Nucl. Mater. 28 (1968) 303.
[22] M.D. Merz, J.H. Hammer, H.E. Kjarmo, J. Nucl. Mater. 51 (1974) 357.
[23] L.J. Wittenberg, R. DeWitt, J. Chem. Phys. 56 (9) (1972) 4526.
[24] V.V. Baidov, M.B. Gitis, Sov. Phys. Semicond. 4 (1970) 825.
[25] M.B. Gitis, I.C. Mikhailov, Sov. Phys. Acoust. 11 (4) (1966) 372.
[26] M.B. Gitis, I.C. Mikhailov, Sov. Phys. Acoust. 12 (1) (1966) 14.
[27] Y. Tsuchiya, J. Phys.: Condens. Matter 3 (1991) 3163.
[28] G. Holton, M.P. Hagelberg, S. Kao, W.H. Johnson, J. Acoust. Soc. Am. 43 (1968) 102.
[29] A. Jayaraman, Phys. Rev. 137 (1965) A179.
[30] S.P. McAlister, E.D. Crozier, Solid State Commun. 40 (1981) 375.
[31] W.H. Zachariasen, J. Inorg. Nucl. Chem. 35 (1973) 3487.
[32] J.L. Smith, E.A. Kmetko, J. Less-Common Met. 90 (1983) 83.
[33] N.G. Cooper, in: Challenges in Plutonium Science, in: Condensed-Matter Physics and Plutonium Aging, vol. 1, Los Alamos Science, Los Alamos, NM, 2000.
[34] J.-L. Truffier, M. Pénicaud, J.-M. Fournier, Clefs C.E.A. (Eds.), Research on Actinides, Commissariat à l'Energie Atomique, 1996.
[35] M. Boivineau, J.-B. Charbonnier, J.-M. Vermeulen, Th. Thévenin, High Press.–High Temp. 25 (1993) 311.